International Journal of Thermal Sciences 48 (2009) 391–400

Contents lists available at ScienceDirect

International Journal of Thermal Sciences

www.elsevier.com/locate/ijts

Study of heat transfer due to laminar flow of copper–water nanofluid through two isothermally heated parallel plates

Apurba Kumar Santra [a,*], Swarnendu Sen [b], Niladri Chakraborty [a]

[a] Department of Power Engineering, Jadavpur University, Salt Lake Campus, Block – LB, Plot-8, Sector – III, Salt Lake, Kolkata 700 098, India
[b] Department of Mechanical Engineering, Jadavpur University, Kolkata 700 032, India

ARTICLE INFO

Article history:
Received 22 January 2008
Received in revised form 10 October 2008
Accepted 13 October 2008
Available online 8 November 2008

Keywords:
Nanofluid
Rectangular duct
Laminar flow
Newtonian
Non-Newtonian

ABSTRACT

Effect of copper–water nanofluid has been studied as a cooling medium to simulate the heat transfer behaviour in a two-dimensional (infinite depth) horizontal rectangular duct, where top and bottom walls are two isothermal symmetric heat sources. The governing continuity, momentum and energy equations for a laminar flow are being discretized using a finite volume approach using a power law profile approximation and has been solved iteratively, through alternate direction implicit, using the SIMPLER algorithm. The thermal conductivity of nanofluid has been determined by model proposed by Patel et al. Study has been conducted considering the fluid as Newtonian as well as non-Newtonian for a wide range of Reynolds number ($Re = 5$ to 1500) and solid volume fraction ($0.00 \leqslant \phi \leqslant 0.050$). It has been observed that the heat transfer augmentation is possible using nanofluid in comparison to conventional fluids for both the cases. The rate of heat transfer increases with the increase in flow as well as increase in solid volume fraction of the nanofluid. Unlike natural convection the increase in heat transfer is almost same for both the cases.

© 2008 Elsevier Masson SAS. All rights reserved.

1. Introduction

Nanofluid is a suspension of solid nanoparticles (1–100 nm diameter) in conventional liquids like water, oil or ethylene glycol. Depending on shape, size, and thermal properties of the solid nanoparticles, the thermal conductivity can be increased by about 40% with low concentration (1–5% by volume) of solid nanoparticle in the mixture [1–3]. The nanofluid is stable [4], introduce very little pressure drop and it can pass through nanochannels. Sometimes stabilizer (e.g., oleic acid and laurate salt) is added with the nanofluid to stabilize the solid particles in the mixture [3,5, 6]. Xuan et al. [3] experimentally obtained thermal conductivity of copper–water nanofluid upto 7.5% of solid volume fraction of 100 nm diameter copper particles. They have also observed that this nanofluid with 5% solid volume fraction remains stable for more than 30 hours without disturbance.

Xuan et al. [7] have examined the transport properties of nanofluid and have expressed that thermal dispersion, which takes place due to the random movement of particles, takes a major role in increasing the heat transfer rate between the fluid and the wall. This requires a thermal dispersion coefficient, which is still unknown. Brownian motion of the particles, ballistic phonon transport through the particles and nanoparticle clustering can also be the possible reason for this enhancement [8]. Das et al. [6] has observed that the thermal conductivity for nanofluid increases with increasing temperature. They have also observed the stability of Al_2O_3–water and CuO–water nanofluid.

Due to lack of sophisticated theory to predict the effective thermal conductivity of nanofluid several researchers have proposed different correlations to predict the apparent thermal conductivity of two-phase mixture. The models proposed by Hamilton and Crosser (HC) [9], Wasp [10], Maxwell-Garnett [11], Bruggeman [12] and Wang et al. [13] to determine the effective thermal conductivity of nanofluid failed to predict it accurately. The experimental results show a much higher thermal conductivity of nanofluid than those predicted by these models. Yu and Choi [14] has proposed a renovated Maxwell model considering the liquid layer thickness, which is proved to be not realistic [15] and it fails to throw light on the temperature dependence of thermal conductivity. Kumar et al. [16] has proposed a model, where effective thermal conductivity is a function of both temperature and particle diameter. Prasher et al. [17] have showed that the enhancement of effective thermal conductivity (k_{eff}) of nanofluid is mainly due to the localized Brownian movement of nanoparticles. They have also proposed a conduction-convection based model to find the k_{eff} of nanofluid. Patel et al. [18] has improved the model given in [16] by incorporating the effect of micro-convection due to particle movement. The effect of temperature is justified as Brownian motion increases with temperature, which causes additional convective effect. The above model is applicable for low concentration of solid volume

* Corresponding author. Tel.: +91 33 2335 5813/ 5215; fax: +91 33 2335 7254.
E-mail address: aksantra@pe.jusl.ac.in (A.K. Santra).

1290-0729/$ – see front matter © 2008 Elsevier Masson SAS. All rights reserved.
doi:10.1016/j.ijthermalsci.2008.10.004

Nomenclature

d	diameter ..... m
g	acceleration due to gravity ..... m/s^2
h, l	height and length of the channel ..... m
H, L	dimensionless height and length of the channel
k	thermal conductivity ..... W/m k
m, n	the respective consistency and fluid behaviour index parameters
Nu_x	local Nusselt number of the heater
$\overline{Nu}$	average Nusselt number at the heater
p	pressure ..... N/m^2
P	dimensionless pressure $p/(\rho_{nf,0}u_\infty^2)$
Pr	Prandtl number of fluid, ν_f/α_f
Re	Reynolds number, $\rho_{f,0}u_\infty h/\mu_{f,0}$
T	temperature ..... K
T_H, T_C	temperature (K) of the heat source and sink respectively
u_∞	free stream velocity at entry of the channel ..... m/s
u, v	velocity components in the x and y directions respectively ..... m/s
U, V	dimensionless velocities ($U = u/u_\infty$, $V = v/u_\infty$)
x, y	horizontal and vertical coordinates respectively .... m
X, Y	dimensionless horizontal and vertical coordinates respectively ($X = x/h$, $Y = y/h$)

Greek symbols

α	thermal diffusivity ..... m^2/s
ϕ	solid volume fraction
μ	dynamic viscosity ..... N s/m^2
ν	kinematic viscosity ..... m^2/s
ρ	density ..... kg/m^3
θ	dimensionless temperature ..... $(T - T_0)/(T_H - T_C)$
ψ	dimensionless stream function
τ	the stress tensor
$\dot{\gamma}$	the symmetric rate of deformation tensor

Subscripts

eff	effective
f	fluid
nf	nanofluid
0	at reference state
s	solid

fraction. Also the model takes into account the effect of particle size through an increase in specific surface are of nanoparticles [19]. There involves an empirical constant 'c', to link the temperature dependence of effective thermal conductivity to the Brownian motion of the particles. This can be found by comparing the calculated value with experimental data, which comes in the order of 10^4. This empirical constant 'c' is adjustable and can be thought as a function of particle properties as well as size [18].

Experiments on heat transfer due to natural convection with nanofluid has been studied by Putra et al. [20] and Wen and Ding [21]. They have observed that heat transfer decreases with increase in concentration of nanoparticles. The viscosity of this nanofluid increases rapidly with inclusion of nanoparticles as shear rate decreases. Recently Santra et al. [22] have numerically investigated the heat transfer in a differentially heated square cavity considering non-Newtonian power law model for copper–water nanofluid. Their findings are similar to that of Refs. [20] and [21].

Several researchers [23–26] have tried to reveal the rheology of nanofluid. Their experiment with different kinds of nanofluid have shown that the well-known viscosity model given by Brinkman [27] is not applicable for nanofluid. They have also shown that viscosity of nanofluid increases with increase in particle solid volume fraction and decrease in mean particle size [24]. Maiga et al. [26] have given a correlation of viscosity of γAl_2O_3–water nanofluid with ϕ which shows that the effective viscosity is much more than predicted by Brinkman model [27]. Heris et al. [28] have carried experiment with Al_2O_3–water and CuO–water nanofluid upto $\phi = 3\%$ and have shown that upto this limit the nanofluid behaves like Newtonian fluid. Above that the viscosity increases rapidly as shear rate decreases. At high shear rate the viscosity becomes constant indicating shear thinning behavior of nanofluid.

Xuan and Li [29] have experimentally investigated the convective heat transfer and flow features of copper–water nanofluid flowing through a tube. They have conducted their study for a wide range of Re (10 000 to 25 000) and ϕ (0.3 to 2%). For turbulent flow ($Re = 10\,000$ to $25\,000$) they have shown that the convective heat transfer coefficient of nanofluid increases with flow velocity as well as ϕ. They have observed about 39% increase in Nusselt number when ϕ was increased from 0 to 2% under same Reynolds number. They have also correlated the Nusselt number as a function of ϕ, Peclet number (Pe), Reynolds number (Re) and Prandtl number (Pr). They presumed that the Pe describes the effect of thermal dispersion. Later Yang et al. [30] have studied experimentally the convective heat transfer of graphite (aspect ratio 0.02) in oil nanofluid for laminar flow in a horizontal tube heat exchanger. They have observed increase in static thermal conductivity of nanofluid. However, increase in heat transfer coefficient was lesser than predicted by the conventional heat transfer correlations. Monsour et al. [31] have studied the effect of the uncertainties in the values of the physical properties of water–γAl_2O_3 nanofluid on their thermo-hydraulic performance for both laminar and turbulent fully developed forced convection in a tube with uniform heat flux. From their study they could not conclude whether has any advantage on heat transfer or not by introducing nanofluid as some properties of nanofluid still not clear. Heris et al. [32] has experimentally investigated laminar flow forced convection heat transfer of Al_2O_3–water nanofluid in a circular tube with constant wall temperature. They have used the renovated Maxwell model [14] to determine the thermal conductivity of the nanofluid with a liquid layer thickness of 10% of the nanoparticle radius. They have found increase in heat transfer with the increase in Peclet number as well as nanoparticle concentration. They have reported that the heat transfer coefficient increases due to presence of nanoparticles, which is much higher than predicted by heat transfer correlation applicable to the single-phase fluid with nanofluid properties. Roy et al. [33] have numerically investigated the effect of water–γAl_2O_3 nanofluid on a radial flow cooling system showing that even two-fold heat transfer enhancement is possible with 10% solid concentration. They have also observed that wall shear stress increases with increase in nanoparticle concentration. Maiga et al. [26] have numerically investigated the hydrodynamic and thermal behavior of γAl_2O_3–water and γAl_2O_3–EG nanofluid flowing inside a uniformly heated tube. For laminar flow a considerable increase in heat transfer has been observed with increase in solid volume fraction with respect to the base fluid. Rate of increase is more for γAl_2O_3–EG nanofluid than γAl_2O_3–water nanofluid. However the wall shear stress also increases rapidly with increase in ϕ. This increase is also more for γAl_2O_3–EG nanofluid.

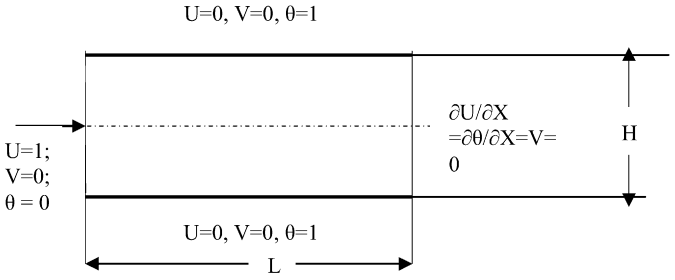

Fig. 1. Geometry of the present problem.

The present paper shows the heat transfer due to laminar flow of copper–water nanofluid through two-dimensional channel with constant temperature walls. Although this type of flow geometry and condition is more pertinent for microchannel flow, there is a dearth of experimental as well as numerical study. We have considered the nanofluid as Newtonian as well as non-Newtonian in nature. To determine the k_{eff} of the nanofluid, model given by Patel et al. [18] has been used with appropriate value of 'c', which has been calculated by matching the experimental result. Since no other model takes care of the temperature dependence of k_{eff}, this model has been considered as best option. The viscosity of nanofluid has been calculated using Brinkman model [27] for Newtonian fluid and Ostwald–de Waele model (two parameter power law model) for a non-Newtonian shear thinning fluid [22]. To the best of the knowledge of the authors, no other numerical study on laminar forced convection using nanofluid particularly considering the fluid as non-Newtonian and the aforesaid thermal conductivity model has been reported so far.

2. Mathematical formulation

2.1. Problem statement

The geometry of the present problem has been shown in Fig. 1. The geometry consists of a two-dimensional rectangular duct of height h and length l. The width of the duct is very large compared to the height. Two symmetric isothermal flush heaters of temperature T_H is mounted on the top wall and bottom wall of the duct. Cold nanofluid of temperature T_C flows from left to the right. As the fluid flows through the duct, it takes away heat from the heat sources placed at the top and bottom. For our case non-dimensional height H $(= h/h)$ is always 1.0 and non-dimensional length L $(= l/h)$ is 100.0 throughout. The nanofluid is a mixture of water and solid spherical copper particles of 100 nm diameter. The nanoparticles are of uniform shape and size. The nanofluid is incompressible and the flow is laminar. Also it is assumed that the liquid and solid are in thermal equilibrium and they flow at same velocity.

The thermophysical properties of the nanofluid are assumed to be constant. In the present case the effect of buoyancy has been neglected, as its effect is not so significant in comparison with the flow.

2.2. Governing equations and boundary conditions

The continuity, momentum and energy equations for a steady, two-dimensional laminar flow has been considered. As the flow is much higher the buoyancy effect has been neglected. The governing equations for a steady, two-dimensional flow are as follows

$$\frac{\partial u}{\partial x}+\frac{\partial v}{\partial y}=0 \tag{1}$$

$$\rho_{nf,o}\left(u\frac{\partial u}{\partial x}+v\frac{\partial u}{\partial y}\right)=-\frac{\partial p}{\partial x}-\left[\frac{\partial \tau_{xx}}{\partial x}+\frac{\partial \tau_{yx}}{\partial y}\right] \tag{2}$$

$$\rho_{nf,o}\left(u\frac{\partial v}{\partial x}+v\frac{\partial v}{\partial y}\right)=-\frac{\partial p}{\partial y}-\left[\frac{\partial \tau_{xy}}{\partial x}+\frac{\partial \tau_{yy}}{\partial y}\right] \tag{3}$$

$$\operatorname{div}(T\vec{v})=\operatorname{div}(\alpha_{nf}\operatorname{grad}T) \tag{4}$$

where $\vec{v}$ is the velocity vector,

$$\alpha_{nf}=\frac{k_{nf}}{(\rho Cp)_{nf,o}} \tag{5}$$

The effective density of the nanofluid at reference temperature is

$$\rho_{nf,0}=(1-\phi)\rho_{f,0}+\phi\rho_{s,0} \tag{6}$$

and the heat capacitance of nanofluid is

$$(\rho Cp)_{nf}=(1-\phi)(\rho Cp)_f+\phi(\rho Cp)_s \tag{7}$$

as given by Xuan et al. [7].

The effective thermal conductivity of fluid has been determined by the model proposed by Patel et al. [18]. For the two-component entity of spherical-particle suspension the model gives

$$\frac{k_{\text{eff}}}{k_f}=1+\frac{k_pA_p}{k_fA_f}+ck_pPe\frac{A_p}{k_fA_f} \tag{8}$$

where

$$\frac{A_p}{A_f}=\frac{d_f}{d_p}\frac{\phi}{(1-\phi)} \tag{9}$$

and

$$Pe=\frac{u_pd_p}{\alpha_f}$$

where u_p is the Brownian motion velocity of the particles which is given by

$$u_p=\frac{2k_bT}{\pi\mu_fd_p^2}$$

where k_b is the Boltzmann constant.

The calculation of effective thermal conductivity can be obtained from Eq. (8).

For an incompressible Newtonian fluid the relationships between the shear stress and shear rate in case of two-dimensional motion in rectangular coordinate are as follows [34]:

$$\tau_{xx}=-2\mu_{nf}\left(\frac{\partial u}{\partial x}\right) \tag{10}$$

$$\tau_{yx}=\tau_{xy}=-\mu_{nf}\left(\frac{\partial u}{\partial y}+\frac{\partial v}{\partial x}\right) \tag{11}$$

$$\tau_{yy}=-2\mu_{nf}\left(\frac{\partial v}{\partial y}\right) \tag{12}$$

Where the effective dynamic viscosity of the nanofluid as given by Brinkman [27] is as follows:

$$\mu_{nf}=\frac{\mu_f}{(1-\phi)^{2.5}} \tag{13}$$

For a non-Newtonian fluid the relationships between the shear stress and shear rate in case of two-dimensional motion in rectangular coordinate according to the Ostwald–de Waele model are as follows [34]:

$$\tau=-m\left[\left|\sqrt{\frac{1}{2}(\dot{\gamma}.\dot{\gamma})}\right|^{(n-1)}\right]\dot{\gamma} \tag{14}$$

where

$$\frac{1}{2}(\dot{\gamma}.\dot{\gamma})=2\left\{\left(\frac{\partial u}{\partial x}\right)^2+\left(\frac{\partial v}{\partial y}\right)^2\right\}+\left(\frac{\partial v}{\partial x}+\frac{\partial u}{\partial y}\right)^2 \tag{15}$$

Thus the stress tensors of Eqs. (2) and (3) take the following forms

Table 1
Values of fluid behavior index parameters (m, n).

Solid volume fraction (ϕ) (%)	m ($\mathrm{N\,sec^n\,m^{-2}}$)	n
0.5	0.00187	0.880
1.0	0.00230	0.830
1.5	0.00283	0.780
2.0	0.00347	0.730
2.5	0.00426	0.680
3.0	0.00535	0.625
3.5	0.00641	0.580
4.0	0.00750	0.540
4.5	0.00876	0.500
5.0	0.01020	0.460

$$\tau_{xx} = -2\left\{m\left|\left[2\left\{\left(\frac{\partial u}{\partial x}\right)^2 + \left(\frac{\partial v}{\partial y}\right)^2\right\} + \left(\frac{\partial v}{\partial x} + \frac{\partial u}{\partial y}\right)^2\right]^{1/2}\right|^{(n-1)}\right\}\left(\frac{\partial u}{\partial x}\right) \tag{16}$$

$$\tau_{yx} = \tau_{xy} = -\left\{m\left|\left[2\left\{\left(\frac{\partial u}{\partial x}\right)^2 + \left(\frac{\partial v}{\partial y}\right)^2\right\} + \left(\frac{\partial v}{\partial x} + \frac{\partial u}{\partial y}\right)^2\right]^{1/2}\right|^{(n-1)}\right\}\left(\frac{\partial u}{\partial y} + \frac{\partial v}{\partial x}\right) \tag{17}$$

$$\tau_{yy} = -2\left\{m\left|\left[2\left\{\left(\frac{\partial u}{\partial x}\right)^2 + \left(\frac{\partial v}{\partial y}\right)^2\right\} + \left(\frac{\partial v}{\partial x} + \frac{\partial u}{\partial y}\right)^2\right]^{1/2}\right|^{(n-1)}\right\}\left(\frac{\partial v}{\partial y}\right) \tag{18}$$

Here m and n are two empirical constants, which depends on the type of nanofluid used. Putra et al. [20] have shown experimentally the relation between the shear stress and shear strain for Al_2O_3–water nanofluid. Using this data, the values of m and n has been calculated for 1% and 4% solid volume fraction. These values are suitably interpolated and extrapolated keeping in mind that the shear stress decreases with increase in ϕ for a particular shear rate in the mixture. The values of m and n for different ϕ has been given in Table 1. It is to be noted that for a shear thinning fluid the value of n is less than 1 [34]. Since the rate of change of shear stress with shear rate for Cu–water nanofluid is not available, these data of Al_2O_3–water nanofluid has been adopted for Cu–water nanofluid to observe the nature of the heat transfer. This approach has already been used in our earlier work [22].

The governing equations can be converted to non-dimensional form, using the following dimensionless parameters

$$X = x/h, \quad Y = y/h, \quad U = u/u_\infty, \quad V = v/u_\infty$$
$$P = p/\left(\rho_{nf,0}\cdot u_\infty^2\right), \quad \text{and } \theta = (T - T_C)/(T_H - T_C) \tag{19}$$

Then the non-dimensional equations for the Newtonian fluid will be as follows:

$$\frac{\partial U}{\partial X} + \frac{\partial V}{\partial Y} = 0 \tag{20}$$

$$U\frac{\partial U}{\partial X} + V\frac{\partial U}{\partial Y} = -\frac{\partial P}{\partial X} + \frac{1.0}{Re}\frac{\rho_{f,0}}{\rho_{nf,0}}\frac{1.0}{(1-\phi)^{2.5}}\left[\frac{\partial^2 U}{\partial X^2} + \frac{\partial^2 U}{\partial Y^2}\right] \tag{21}$$

$$U\frac{\partial V}{\partial X} + V\frac{\partial V}{\partial Y} = -\frac{\partial P}{\partial Y} + \frac{1.0}{Re}\frac{\rho_{f,0}}{\rho_{nf,0}}\frac{1.0}{(1-\phi)^{2.5}}\left[\frac{\partial^2 V}{\partial X^2} + \frac{\partial^2 V}{\partial Y^2}\right] \tag{22}$$

$$\mathrm{div}(\theta\vec{V}) = \mathrm{div}\left(\frac{k_{nf}}{k_f}\frac{(\rho Cp)_{f,0}}{(\rho Cp)_{nf,0}}\frac{1.0}{Re\,Pr}\,\mathrm{grad}\,\theta\right) \tag{23}$$

Where as for non-Newtonian fluid the non-dimensional form of Eqs. (2) and (3) will take the following shape:

$$U\frac{\partial U}{\partial X} + V\frac{\partial U}{\partial Y} = -\frac{\partial P}{\partial X} + m\frac{U_\infty^{n-2}}{h^n}\left|\left[2\left\{\left(\frac{\partial U}{\partial X}\right)^2 + \left(\frac{\partial V}{\partial Y}\right)^2\right\} + \left(\frac{\partial V}{\partial X} + \frac{\partial U}{\partial Y}\right)^2\right]^{1/2}\right|^{(n-1)}\left[\frac{\partial^2 U}{\partial X^2} + \frac{\partial^2 U}{\partial Y^2}\right] \tag{24}$$

$$U\frac{\partial V}{\partial X} + V\frac{\partial V}{\partial Y} = -\frac{\partial P}{\partial Y} + m\frac{U_\infty^{n-2}}{h^n}\left|\left[2\left\{\left(\frac{\partial U}{\partial X}\right)^2 + \left(\frac{\partial V}{\partial Y}\right)^2\right\} + \left(\frac{\partial V}{\partial X} + \frac{\partial U}{\partial Y}\right)^2\right]^{1/2}\right|^{(n-1)}\left[\frac{\partial^2 V}{\partial X^2} + \frac{\partial^2 V}{\partial Y^2}\right] \tag{25}$$

while Eqs. (1) and (4) will be same as of Eqs. (20) and (23), respectively.

The boundary conditions, used to solve Eqs. (20) to (25) are as follows

$u = u_\infty, \quad v = 0, \quad T = T_C$

at $x = 0$ and $0 \leqslant y \leqslant h$; i.e.

$U = 1.0, \quad V = \theta = 0$

at $X = 0$ and $0 \leqslant Y \leqslant H$

$\dfrac{\partial u}{\partial x} = v = \dfrac{\partial T}{\partial x} = 0$

at $x = l$ and $0 \leqslant y \leqslant h$; i.e.

$\dfrac{\partial U}{\partial X} = V = \dfrac{\partial \theta}{\partial X} = 0$

at $X = L$ and $0 \leqslant Y \leqslant H$

$u = v = 0, \quad T = T_H$

at $y = 0$, $y = h$ and $0 \leqslant x \leqslant l$; i.e.

$\theta = 1.0$ and $U = V = 0$

at $Y = 0$, $Y = H$ and $0 \leqslant X \leqslant L$

Eqs. (20) to (25), along with the boundary conditions are solved numerically. From the converged solutions, we have calculated Nu_x (local Nusselt number) and $\overline{Nu}$ (average Nusselt number) for the bottom hot wall as follows

$$Nu_x = -\frac{k_{nf}}{k_f}\frac{\partial \theta}{\partial Y}\bigg|_{X,0} \tag{26}$$

$$\overline{Nu} = -\frac{1}{L}\int_0^L Nu_x\,dX|_{Y=0} \tag{27}$$

In a similar fashion the local and the average Nusselt number of the top hot wall has been determined. We have defined the dimensionless stream function ψ as $U = \partial\psi/\partial Y$ and $V = -\partial\psi/\partial X$. The stream function at and grid location (X, Y) is calculated as

$$\psi(X, Y) = \int_{Y_0}^{Y} U\cdot\partial Y + \psi(X, Y_0) \tag{28}$$

Along the solid boundary the stream function is taken as zero. $\psi(X, Y_0)$ is known either from the previous calculation, or, from the boundary condition.

The non-dimensional shear stress at the wall has been calculated as

$$\tau_{\mathrm{wall}} = \frac{\mu_{\mathrm{app}}}{\mu_f}\frac{\partial U}{\partial Y}\bigg|_{\mathrm{wall}} \tag{29}$$

Table 2
Results of grid independence test.

No. of grids in X-direction	No. of grids in Y-direction	Average Nusselt number at the bottom wall	Average wall shear stress
401	21	7.14309	7.074227
501	21	7.14224	7.073601
601	21	7.14168	7.073185
701	21	7.14129	7.072887
801	21	7.14100	7.07266
201	31	7.09640	7.101937
301	31	7.09320	7.099266
401	31	7.09159	7.098041
501	31	7.09062	7.097301
401	41	7.07098	7.118145

Table 3
Fully developed length for clear fluid ($\phi = 0.0\%$) for different Reynolds number.

Re	Present study	Durst et al. [36]	% deviation
5	0.711535	0.702225	1.325833
10	0.813569	0.835087	−2.5768
20	1.204162	1.177987	2.222022
50	2.569990	2.391482	7.464329
200	9.549150	8.920699	7.04486
100	4.927244	4.541651	8.490152
500	23.208660	22.14667	4.795269
1000	45.685680	44.2308	3.289286
1500	68.040540	66.32415	2.587876

3. Numerical approach

The governing mass, momentum and energy equations has been discretized by a control volume approach using a power law profile approximation. The set of discretized equations have been solved iteratively, through alternate direction implicit ADI method, using the SIMPLER algorithm [35]. To save computational time we have taken the half of the domain as computational domain as the problem is symmetric in nature. To achieve convergence, for pressure velocity coupling under-relaxation of velocities and pressure has been employed. To check the convergence, the mass residue of each control volume has been calculated using double precision and the maximum value has been used to check the convergence. The grids are non-uniform. Grids are finer near the boundaries while coarser at the core region. The convergence criterion has been set to 10^{-7}. It is observed that $\overline{Nu}$ remains unchanged up to the fourth place of decimal if the convergence criterion is further lowered by a factor of ten.

4. Grid independence study

A grid independence study has been conducted for the half domain and increase in average Nusselt number as well as average wall shear stress have been calculated. It is found that 401 (along x-direction) by 31 nodes (along y-direction) gives the best result. With further increase in the number of grids do not affect the result. The result of the grid independence study has been summarized in Table 2.

5. Validation of code

The fully developed length for clear fluid (water) has been calculated and has been compared with the correlation given by Durst et al. [36]. The results has been summarized in Table 3. It has been observed that the percentage deviation in fully developed length is very less when compared with that obtained from the correlations given in Ref. [36]. Further is has been observed that the flow of the present study, is hydrodynamically fully developed but do not achieve the thermal development. The local non-dimensional wall shear stress for clear fluid (i.e., $\phi = 0$) in the fully developed zone is coming as about 6.0 which is exactly same with that of theoretical wall shear stress [37] for flow of a Newtonian fluid through two-dimensional channel. No other study about non-Newtonian study through two-dimensional channel has been found to validate the code.

Table 4
Thermophysical properties of different phase at 20 °C.

Property	Fluid (water)	Solid (copper)
C_p (J/kg K)	4181.80	383.1
ρ (kg/m^3)	1000.52	8954.0
k (W/m K)	0.597	386.0
β (K^{-1})	210.0×10^{-6}	51.0×10^{-6}

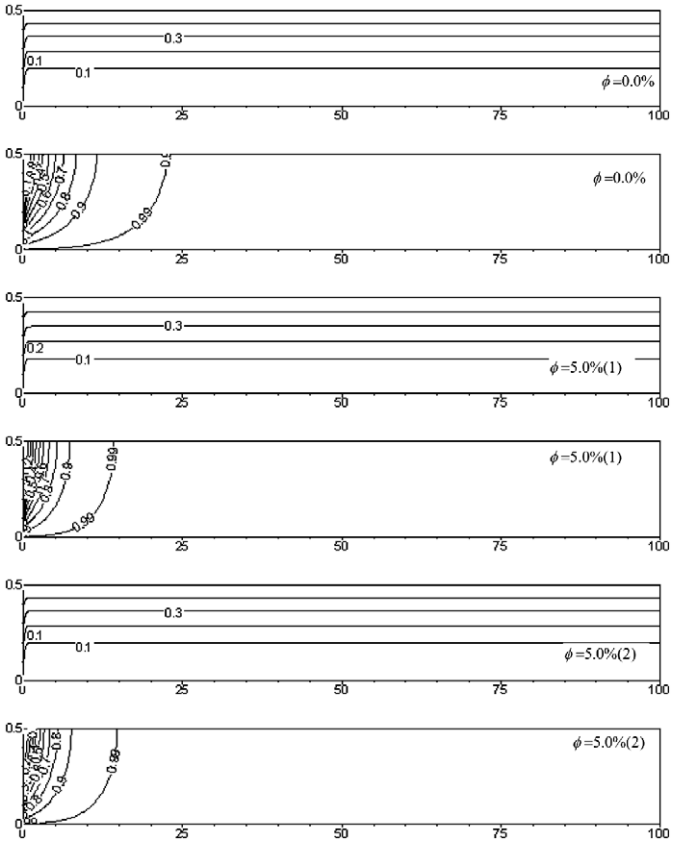

Fig. 2. Streamlines and isotherms for $Re = 5$. (1) Non-Newtonian, (2) Newtonian.

6. Results and discussion

The heat transfer problems associated with the flow of nanofluid through a two-dimensional rectangular duct has been studied numerically where two symmetric isothermal heaters have been placed on the walls. Geometry of the problem has been shown in Fig. 1. The length of the duct is 100 times that of the height.

The flow and heat transfer for a range of Re and ϕ have been studied. Water has been considered as the base fluid with $Pr = 7.02$ (considering base temperature as 20 °C) [38], for the present study. Solid spherical copper nanoparticles of 100 nm diameter mixed with water, has been considered as nanofluid. The effective thermal conductivity of nanofluid has been calculated using the correlation given in [18] for each control volume as the k_{eff} is temperature dependent. The constant 'c' which appears in the correlation has been calculated from the experimental data available for copper water nanofluid [3]. The average value of constant has been considered for our simulation, which came out as 3.60×10^4 that is in line with result given in Ref. [18]. The phys-

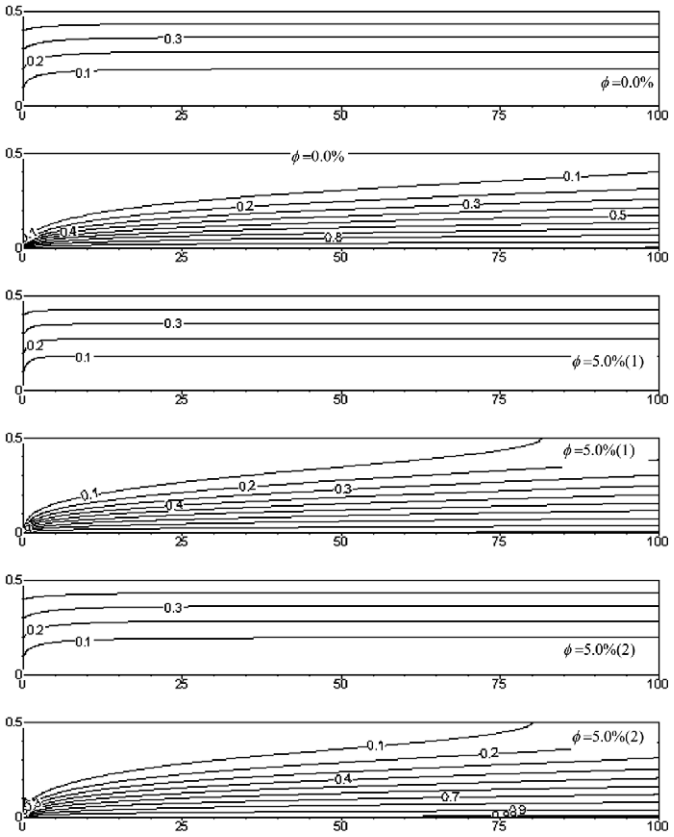

Fig. 3. Streamlines and isotherms for $Re = 500$. (1) Non-Newtonian, (2) Newtonian.

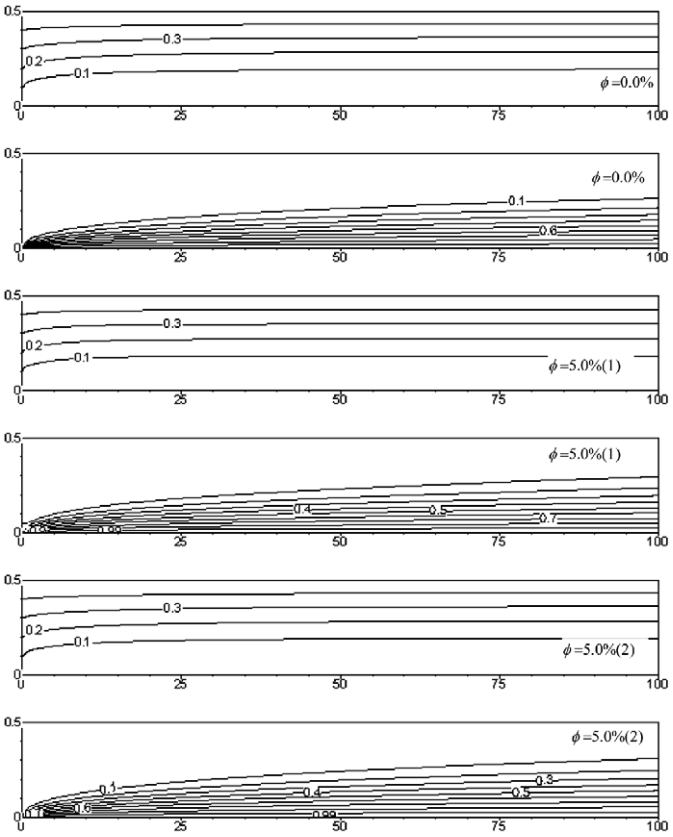

Fig. 4. Streamlines and isotherms for $Re = 1500$. (1) Non-Newtonian, (2) Newtonian.

ical and thermal properties of both the solid and the fluid at the base temperature, i.e. at 20 °C have been summarized in Table 4 [38,39]. The constants m and n for calculating shear stresses have been taken from the experimental observation [20] and has been given in Table 1. Results are presented for $Re = 5$ to 1500, while ϕ has been varied from 0.0 to 5.0% with the increment of 0.5%. The hot wall temperature has been considered as 303 K (30 °C) while the cold wall temperature is 293 K (20 °C).

6.1. Effect of solid volume fraction on streamlines and isotherms

Since, the heat transfer is strongly affected by the nature of flow, and the thermal properties of fluid, the flow structure and isotherms have been considered before discussing the variation of Nusselt number with different parameters.

The flow patterns and isotherms for $\phi = 0\%$ and $\phi = 5\%$ for both the non-Newtonian (denoted as 1) and Newtonian (denoted as 2) nanofluid for $Re = 5$, 500 and 1500 has been shown in Figs. 2, 3 and 4, respectively. The streamlines shows that there are no such appreciable change in flow pattern for a particular Re, with increase in the ϕ. The flow becomes fully developed after the entry length. The developing flow length remains almost same with increase in ϕ. The isotherms show that for a particular Re the isotherms shifts towards centre of the duct as ϕ increases. That is, the thermal boundary layer at particular X increases rapidly as ϕ increases. Though the term $\partial\theta/\partial Y$ decrease with increase in ϕ, but the overall heat transfer increases with ϕ, as the effective thermal conductivity of the nanofluid increases with ϕ. From Fig. 2 it is clear that for $Re = 5$ the flow is thermally fully developed at the exit of the channel where diffusion is much higher than convection. For higher Reynolds number (Figs. 3 and 4) the flow remains thermally developing at the exit of the channel, because convection dominates over diffusion. Considering the flow structures and the isotherms of a Newtonian and a non-Newtonian nanofluid (in Figs. 2, 3, and 4) we find that for non-Newtonian flow the entry length is much higher than Newtonian flow possibly be due to high viscosity of the non-Newtonian fluid. For the isotherms it is observed that the thermal boundary layer thickness for Newtonian fluid is slightly more than that of non-Newtonian approach. Thus the term $\partial\theta/\partial Y$ is more for non-Newtonian flow than Newtonian flow. Since effective thermal conductivity remains same for both the cases, heat transfer is slightly higher for non-Newtonian model. But the difference is very small. This may be due the shear thinning nature of nanofluid where effective viscosity becomes almost constant at high shear rate [28]. This feature is common for any Reynolds number. It may be noted that at higher Re, any shear thinning fluid behaves like Newtonian fluid and the thermal boundary layer should be same for both the cases. This discrepancy may be due to choosing of models, because actual behavior of viscosity of copper–water nanofluid is still unknown.

6.2. Effect of solid volume fraction on wall shear stress

The variation of the average wall shear stress for different Re and ϕ for both Newtonian and non-Newtonian nanofluids, along the hot wall for the hydrodynamically fully developed region has been plotted in Fig. 5. For this purpose non-dimensional length of 30 has been taken after the flow becomes hydrodynamically fully developed. It shows that with increase in ϕ the average wall shear stress increases with reference to the base fluid for a non-Newtonian fluid. This outcome is similar to that obtained by Maiga et al. [26] for laminar forced convection through pipes. For a particular ϕ wall shear stress decreases with increase in Re. For $Re = 1000$ there is almost no change in wall shear stress with ϕ, for $Re = 1500$ it decreases with ϕ. When the fluid is considered as Newtonian almost no change in average wall shear stress has been observed either with change in Re or in ϕ.

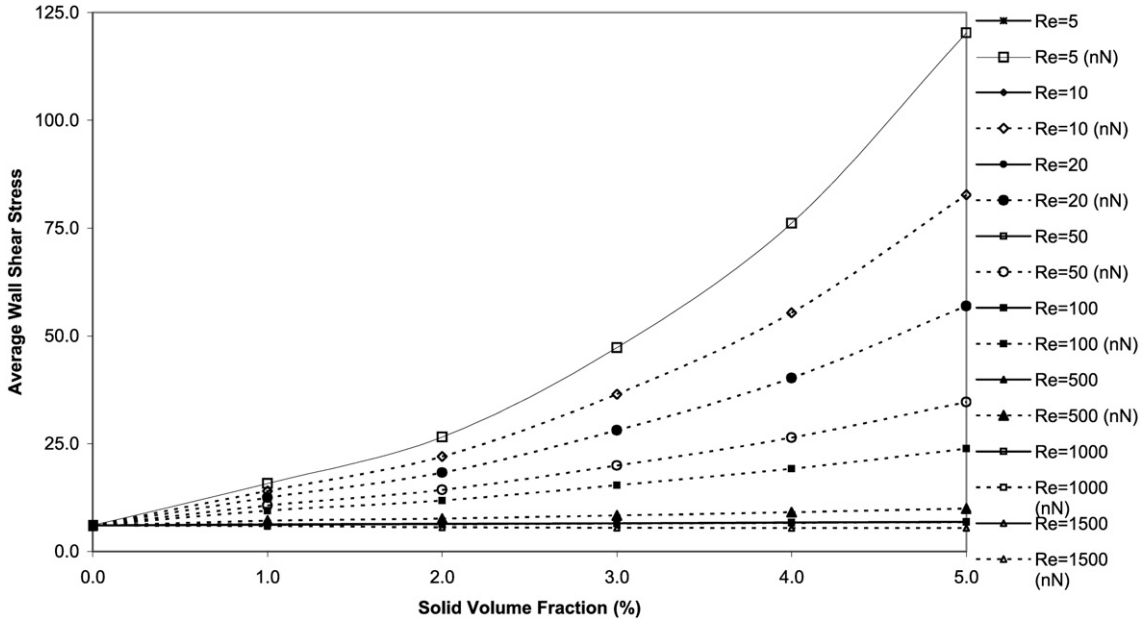

Fig. 5. Average wall shear stress for different Reynolds number and ϕ for fully developed zone.

Table 5
Percentage increase in $\overline{Nu}$ with respect to the clear fluid for different Re and ϕ (N = Newtonian consideration, n-N = non-Newtonian consideration).

ϕ (%)	$Re = 100.0$ (N)	$Re = 100.0$ (n-N)	$Re = 500.0$ (N)	$Re = 500.0$ (n-N)	$Re = 1000.0$ (N)	$Re = 1000.0$ (n-N)	$Re = 1500.0$ (N)	$Re = 1500.0$ (n-N)
0.0	0.00000	0.00000	0.00000	0.00000	0.00000	0.00000	0.00000	0.00000
0.5	2.33984	2.46569	3.21628	3.05237	3.26732	2.77872	3.30307	2.59473
1.0	4.57419	4.80181	6.40564	6.34507	6.51014	6.08204	6.58250	5.92820
1.5	6.70601	7.05901	9.56952	9.68160	9.72955	9.45015	9.83894	9.34089
2.0	8.73821	9.24055	12.70968	13.07662	12.92740	12.90516	13.07415	12.86227
2.5	10.67540	11.34941	15.82767	16.53598	16.10541	16.44816	16.28976	16.48784
3.0	12.51881	13.41280	18.92487	20.11710	19.26517	20.14111	19.48727	20.28067
3.5	14.27220	15.36718	22.00248	23.70964	22.40813	23.88314	22.66808	24.14623
4.0	15.93857	17.22629	25.06157	27.32893	25.53565	27.68259	25.83347	28.08796
4.5	17.52087	19.01697	28.10305	31.03210	28.64899	31.60195	28.98467	32.16896
5.0	19.02200	20.73696	31.12774	34.83734	31.74931	35.66481	32.12279	36.41625

The wall shear distribution has been shown for different Re and ϕ for both Newtonian and non-Newtonian nanofluid has been shown in Fig. 6. In Fig. 6(a) the wall shear for $Re = 5$ for different ϕ has been shown. The distribution shows that the wall shear stress near developing and developed zone is much higher for non-Newtonian case for any ϕ, which is highest for $\phi = 5.0\%$ and gradually decreases with decrease in ϕ. But for Newtonian case it is same for any ϕ. This is due to the fact that at low Re the shear rate is low, so non-Newtonian fluid has much higher viscosity that Newtonian fluid. The same for $Re = 1500$ and $Re = 500$ has been shown in Figs. 6(b) and 6(c), respectively. For $Re = 1500$ wall shear stress for non-Newtonian fluid is less than Newtonian nanofluid for any ϕ. It is minimum for $\phi = 5\%$. While for $Re = 500$ [Fig. 6(c)] there is a transition from developing to fully developed condition. Initially at the entrance section the shear stress for non-Newtonian cases are higher and as the flow develops gradually the shear stress for Newtonian fluid becomes lesser than non-Newtonian fluid. So it can be presumed from Figs. 6(b) and 6(c) that after a certain Reynolds number non-Newtonian fluid will have less shear stress than non-Newtonian fluid. Fig. 6(d) presents the wall shear stress for $\phi = 2.5\%$ for $Re = 100$, 500, and 1500. From this figure it is again confirmed that for lower Re non-Newtonian fluid has higher wall shear than Newtonian fluid while as Re increases a transition occurs and after $Re = 500$ non-Newtonian fluid has lower shear rate than Newtonian fluid. This feature is same or any other ϕ. Hence it can be stated that at higher Re the pumping power required for nanofluid will be less than Newtonian fluid.

6.3. Effect of solid volume fraction on average Nusselt number

The variation of the average Nusselt number ($\overline{Nu}$) along the hot wall has been presented in Fig. 7 for different Re and ϕ for both Newtonian and non-Newtonian nanofluids. The figure shows that $\overline{Nu}$ increases with increase in Re as well ϕ. This is due to the increase in effective thermal conductivity of the nanofluid with increase in ϕ as well as increase in convection with the increase in Re. This is contrary to the results obtained in case of natural convection, where heat transfer decreases with increase in ϕ [20–22] when fluid is considered as non-Newtonian. Here, the results are similar to that observed by Xuan and Li [29] and Heris et al. [32]. The heat transfer for non-Newtonian fluid is slightly higher than the Newtonian fluid for higher Re. This difference increases with ϕ. This indicates that for laminar forced flow condition the shear rate is much higher and a shear thinning fluid behaves like Newtonian fluid at high shear rate [28]. The percentage increase in $\overline{Nu}$ with respect to the clear fluid has been listed in Table 5 for higher Re and ϕ for both the Newtonian and non-Newtonian considerations. The heat transfer increases with increase in ϕ. It shows that the percentage increase in $\overline{Nu}$ for non-Newtonian nanofluid is slightly higher that Newtonian nanofluid. Also it has been observed that

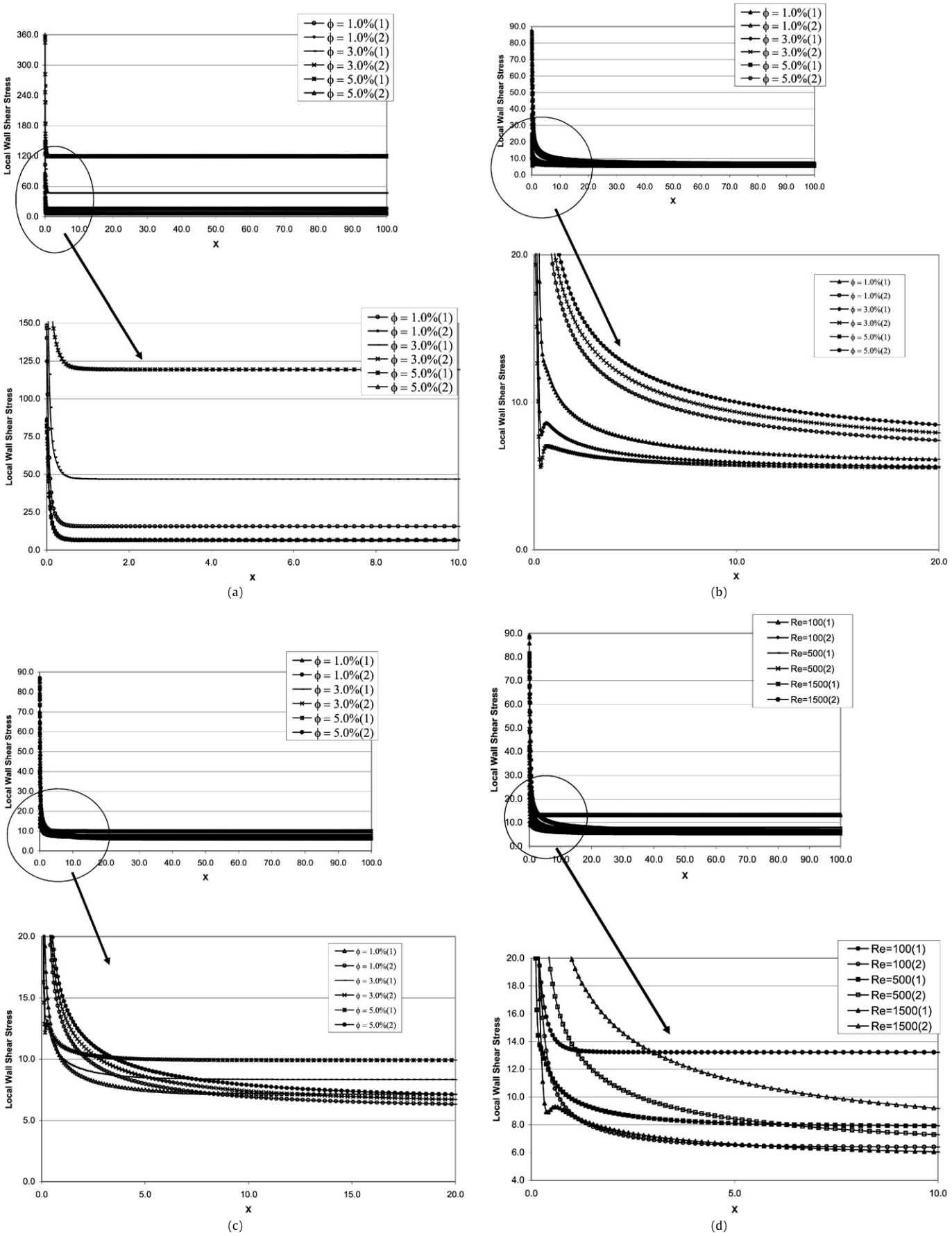

Fig. 6. Distribution of local shear stress for both Newtonian and non-Newtonian nanofluid for (a) $Re = 5$, (b) $Re = 1500$, (c) $Re = 500$, (d) $\phi = 2.5\%$. (1) Non-Newtonian, (2) Newtonian.

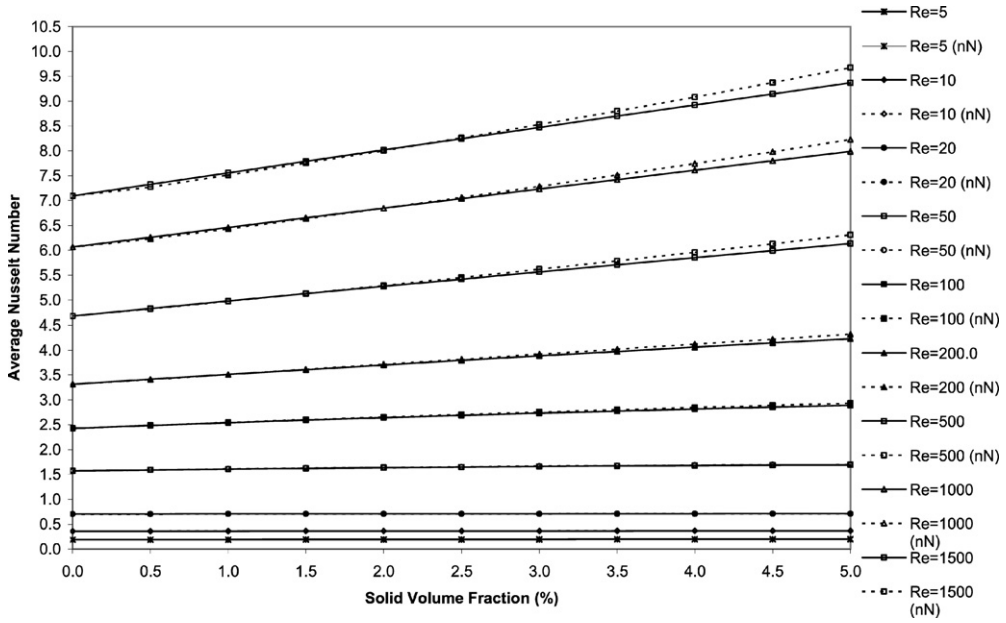

Fig. 7. Average Nusselt number at hot wall for different Reynolds number and ϕ.

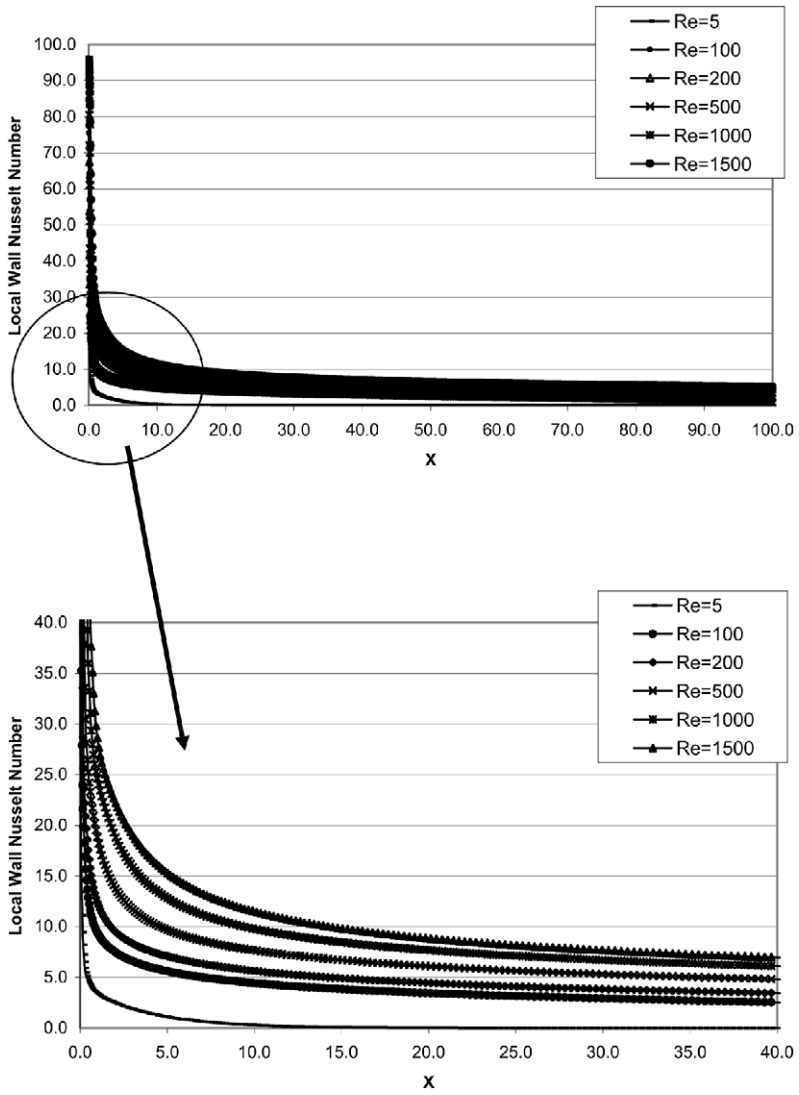

Fig. 8. Distribution of local Nusselt number at hot wall for non-Newtonian nanofluid for $\phi = 2.5\%$.

the percentage of heat transfer for a particular ϕ, increases with increase in *Re*.

Fig. 8 shows the local Nusselt numbers at the wall for $\phi = 2.5\%$ for different Reynolds number for non-Newtonian nanofluid. The figure shows that the local Nusselt number decreases rapidly as the flow proceeds. After a certain length the local Nusselt number at the wall becomes almost constant. For $Re = 5$ it becomes constant rapidly and flow becomes thermally fully developed, For higher *Re* the flow is still developing at the exit of the channel. This feature is same for both non-Newtonian and Newtonian nanofluid for any ϕ.

7. Conclusions

Heat transfer enhancement due to flow of copper–water nanofluid through a two-dimensional rectangular duct has been studied for a range of Reynolds number ($5 \leqslant Re \leqslant 1500$) with a wide range of solid volume fraction ($0.00 \leqslant \phi \leqslant 0.050$). The nanofluid has been considered as Newtonian as well as non-Newtonian in nature. The diameter of copper particle is 100 nm and Prandtl number of clear fluid is 7.02. The Ostwald–de Waele model for a non-Newtonian shear thinning fluid has been considered to calculate shear stresses of the non-Newtonian nanofluid. The constants for model have been taken from the experiment of Putra et al. [18]. For Newtonian nanofluid Brinkman model [27] has been used to determine the effective viscosity of nanofluid. The effective thermal conductivity of the nanofluids has been predicted using the model proposed by Patel et al. [18]. The numerical analysis has been performed using primitive variables. The result shows that there is a little effect of nanoparticles on the flow structure but the isotherms changes and it moves towards centerline of the channel with increase in solid volume fraction. The results also show a considerable increase in heat transfer for increase in solid volume fraction for any Reynolds number. This increment is more or less same for both the Newtonian and non-Newtonian nanofluid, particularly for lower *Re*. The nature of local Nusselt number distribution at the wall is similar for non-Newtonian and Newtonian nanofluid for any ϕ. For non-Newtonian nanofluid the wall shear stress increases rapidly with increase in solid volume fraction for lower *Re* while the rate of increase decreases as *Re* increases. At $Re = 1500$ the wall shear stress decreases with ϕ, which indicates that less pumping power is required with non-Newtonian fluid than Newtonian fluid. Local shear distribution at wall shows that at lower *Re* non-Newtonian fluid imparts more shear than Newtonian fluid. However as *Re* increases the difference decreases and at higher *Re* it becomes less than Newtonian fluid. There is critical Reynolds number where this transition occurs.

References

[1] S. Lee, S.U.S. Choi, S. Li, J.A. Eastman, Measuring thermal conductivity of fluids containing oxide nanoparticles, Trans. ASME J. Heat Transfer 121 (1999) 280–289.

[2] J.A. Eastman, S.U.S. Choi, S. Li, W. Yu, L.J. Thompson, Anomalously increased effective thermal conductivities of ethylene glycol-based nanofluids containing copper nanoparticles, Appl. Phys. Lett. 78 (2001) 718–720.

[3] Y. Xuan, Q. Li, Heat transfer enhancement of nanofluids, Int. J. Heat Fluid Flow 21 (2000) 58–64.

[4] D.W. Zhou, Heat transfer enhancement of copper nanofluid with acoustic cavitation, Int. J. Heat Mass Transfer 47 (2004) 3109–3117.

[5] H.E. Patel, S.K. Das, T. Sundarrajan, A.S. Nair, B. George, T. Pradeep, Thermal conductivities of naked and monolayer protected metal nanoparticle based nanofluids: Manifestation of anomalous enhancement and chemical effects, Appl. Phys. Lett. 83 (2003) 2931–2933.

[6] S.K. Das, N. Putra, P. Thiesen, W. Roetzel, Temperature dependence of thermal conductivity enhancement for nanofluids, J. Heat Transfer 125 (2003) 567–574.

[7] Y. Xuan, W. Roetzel, Conceptions for heat transfer correlation of nanofluids, Int. J. Heat Mass Transfer 43 (2000) 3701–3707.

[8] P. Keblinski, S.R. Phillpot, S.U.S. Choi, J.A. Eastman, Mechanisms of heat flow in suspensions of nano-sized particles (nanofluids), Int. J. Heat Mass Transfer 45 (2002) 855–863.

[9] R.L. Hamilton, O.K. Crosser, Thermal conductivity of heterogeneous two-component systems, I & EC Fundamentals 1 (1962) 182–191.

[10] F.J. Wasp, Solid–Liquid Flow Slurry Pipeline Transportation, Trans. Tech. Pub., Berlin, 1977.

[11] J.C. Maxwell-Garnett, Colours in metal glasses and in metallic films, Philos. Trans. Roy. Soc. A 203 (1904) 385–420.

[12] D.A.G. Bruggeman, Berechnung Verschiedener Physikalischer Konstanten von Heterogenen Substanzen, I. Dielektrizitatskonstanten und Leitfahigkeiten der Mischkorper aus Isotropen Substanzen, Annalen der Physik. Leipzig 24 (1935) 636–679.

[13] B.X. Wang, L.P. Zhou, X.F. Peng, A fractal model for predicting the effective thermal conductivity of liquid with suspension of nanoparticles, Int. J. Heat Mass Transfer 46 (2003) 2665–2672.

[14] W. Yu, S.U.S. Choi, The role of interfacial layer in the enhanced thermal conductivity of nanofluids: A renovated Maxwell model, J. Nanoparticles Res. (2003) 167–171.

[15] L. Xue, P. Keblinski, S.R. Phillpot, S.U.S. Choi, A.J. Eastman, Effect of liquid layering at the liquid–solid interface on thermal transport, Int. J. Heat Mass Transfer 47 (2004) 4277–4284.

[16] D.H. Kumar, H.E. Patel, V.R.R. Kumar, T. Sundararajan, T. Pradeep, S.K. Das, Model for conduction in nanofluids, Phys. Rev. Lett. 93 (2004) 144301-1–144301-4.

[17] R. Prasher, P. Bhattacharya, P.E. Phelan, Brownian-motion-based convective-conductive model for the effective thermal conductivity of nanofluid, ASME J. Heat Transfer 128 (2006) 588–595.

[18] H.E. Patel, T. Pradeep, T. Sundarrajan, A. Dasgupta, N. Dasgupta, S.K. Das, A micro-convection model for thermal conductivity of nanofluid, Pramana–J. Phys. 65 (2005) 863–869.

[19] S.K. Das, et al., Reply, Phys. Rev. Lett. 95 (2005) 019402.

[20] N. Putra, W. Roetzel, S.K. Das, Natural convection of nano-fluids, Heat Mass Transfer 39 (2003) 775–784.

[21] D. Wen, Y. Ding, Natural convective heat transfer of suspensions of titanium dioxide nanoparticles (nanofluids), IEEE Trans. Nanotechnol. 5 (2006) 220–227.

[22] A.K. Santra, S. Sen, N. Chakraborty, Study of heat transfer augmentation in a differentially heated square cavity using copper–water nanofluid, Int. J. Thermal Sci. 47 (2008) 1113–1122.

[23] K. Kwak, C. Kim, Viscosity and thermal conductivity of copper oxide nanofluid dispersed in ethylene glycol, Korea–Australia Rheol. J. 17 (2005) 35–40.

[24] H. Chang, C.S. Jwo, C.H. Lo, T.T. Tsung, M.J. Kao, H.M. Lin, Rheology of CuO nanoparticle suspension prepared by ASNSS, Rev. Adv. Material Sci. 10 (2005) 128–132.

[25] Y. Ding, H. Alias, D. Wen, R.A. Williams, Heat transfer of aqueous suspensions of carbon nanotubes (CNT nanofluids), Int. J. Heat Mass Transfer 49 (2006) 240–250.

[26] S.E.B. Maiga, C.T. Nguyen, N. Galanis, G. Roy, Heat transfer behaviours of nanofluids in a uniformly heated tube, Superlattices and Microstructures 35 (2004) 543–557.

[27] H.C. Brinkman, The viscosity of concentrated suspensions and solutions, J. Chem. Phys. 20 (1952) 571–581.

[28] S.Z. Heris, S.Gh. Etemad, M.N. Esfahany, Experimental investigation of oxide nanofluids laminar flow convective heat transfer, Int. Comm. Heat Mass Transfer 33 (2006) 529–535.

[29] Y. Xuan, Q. Li, Investigation on convective heat transfer and flow features of nanofluids, J. Heat Transfer 125 (2003) 151–155.

[30] Y. Yang, Z.G. Zhang, A.R. Grukle, W.B. Anderson, G. Wu, Heat transfer properties of nanoparticle-in-fluid dispersions (nanofluids) in laminar flow, Int. J. Heat Mass Transfer 48 (2005) 1107–1116.

[31] B.R. Monsour, Galanis, C.T. Nguyen, Effect of uncertainties in physical properties on forced convection heat transfer with nanofluids, Appl. Thermal Engrg. 27 (2007) 240–249.

[32] S.Z. Heris, M.N. Esfahany, S.Gh. Etemad, Experimental investigation of convective heat transfer of Al_2O_3/water nanofluid in circular tube, Int. J. Heat Fluid Flow 28 (2007) 203–210.

[33] G. Roy, C.T. Nguyen, P.-R. Lajoie, Numerical investigation of laminar flow and heat transfer in a radial flow cooling system with the use of nanofluids, Superlattices and Microstructures 35 (2004) 497–511.

[34] R.B. Bird, W.E. Stewert, E.N. Lightfoot, Transport Phenomena, John Wiley & Sons, Singapore, 1960.

[35] S.V. Patankar, Numerical Heat Transfer and Fluid Flow, Hemisphere, Washington D.C., 1980.

[36] F. Durst, S. Ray, B. Unsal, O.A. Bayoumi, The development lengths of laminar pipe and channel flows, ASME J. Fluids Engrg. 127 (2005) 1154–1160.

[37] L.C. Burmeister, Convective Heat Transfer, John Wiely & Sons, USA, 1983.

[38] M.N. Ozisik, Heat Transfer—A Basic Approach, McGrawhill International Edition, 1985.

[39] Website of Western Washington University, Bellingham, Washington, http://www.ac.wwu.edu/~vawter/PhysicsNet/Topics/Thermal/ThermExpan.htm.